

The Effects of Electrode Configuration on Body Channel Communication Based on Analysis of Vertical and Horizontal Electric Dipoles

Joonsung Bae, *Member, IEEE*, and Hoi-Jun Yoo, *Fellow, IEEE*

Abstract—The effects of electrode configuration on body channel communication (BCC) are studied for the development of body channel characteristics, such as frequency response, path loss, and resilience to other interferers. First, this paper introduces nine types of electrode configurations according to the arrangement and direction of both transmitting and receiving electrodes on the body. Each configuration is then modeled by means of vertical and horizontal electric dipoles. From Maxwell's equations, the complete equations of vertical and horizontal electric fields on the human body, followed by the ratios of the received electric field to the transmitted electric field, are obtained to find the theoretical body channel characteristics and the effect of electrode configurations on the body channel. The theory is verified with measurement results using a network analyzer and balun transformer. In addition to the channel characteristics, the influence of BCC and RF interference on the body channel is investigated and discussed along with receiving electrode configurations. Based on the measurement results, we found that vertical electrodes in the transmitter and horizontal electrodes with longitudinal direction in the receiver is the optimal configuration for BCC in regard to transmission gain, environmental sensitivity, and interference resilience. Finally, we suggest an effective parameter for BCC, which is equivalent reference distance to determine the proper electrode size for the required frequency response. The relation between the parameter and the electrode size is formulated for the purpose of proper electrode utilization in the design of BCC systems as well as in many potential applications.

Index Terms—Body channel communication (BCC), electric field, electrode configuration, horizontal dipole, human body communication (HBC), interference, intra-body communication, on-body transmission, surface wave, vertical dipole.

I. INTRODUCTION

RECENT achievements in information and communication technology (ICT) enable the new paradigm of the Internet of Things (IoT), in which everything is interconnected through the World Wide Web [1]. The IoT sheds new light on the short-range connectivity among various physiological sensors and wearable devices carried by human bodies for

continuous and ambulatory connection. The wireless body area network (WBAN) is an optimal network system around the human body for longer battery lifetime due to the short communication distance (< 2 m) [2]. The IEEE 802.15.6 (WBAN) standard [3] is composed of a common media access control layer (MAC), which supports scalable quality of service (QoS) and the three physical layers (PHY), which are ultra-wideband (UWB) PHY, narrowband (NB) PHY, and body channel communication (BCC) PHY. While the NB and UWB PHY are to provide highly reliable wireless communication and a high data rate, the BCC PHY mainly focuses on energy efficiency due to the low path loss thanks to the high conductivity of the human body. BCC utilizes the surface of the human body to send the electric signals with a pair of electrodes, and the potential difference is sensed by the electrode pair on the other side of the body. The low energy consumption of a BCC transceiver (TRX) has been proven in a variety of previous implementations [4]–[6] and standard document of IEEE 802.15.6 [3].

Nevertheless, compared to the RF communications of NB and UWB PHY, which propagate through air channels with antenna interfaces, the understanding of the BCC communication mechanism has not been well established, especially in the interface between the human body and electrodes. There has been a lack of research on the electrical property of the electrode interface, even in the standard document [3]. This is because most BCC research has focused on describing the measurement [7], [8] or analysis based on simulation results [9] with a phenomenological approach, without a clear understanding of physical principles behind BCC. While the analysis for the body channel characteristics has been thoroughly investigated in [10], which has a limitation in that only a vertical electrode was assumed and exploited, the effects of other electrode configurations on BCC were not considered at all. Just as the configuration or utilization of the antenna, such as whether it is a monopole or a dipole, has a significant effect on the communication [11], it is straightforward that the configuration or utilization of the electrodes is the most important consideration in BCC characteristics and design of BCC systems. Therefore, in this paper, the effects of electrode configurations on BCC are studied for the development of the body channel characteristics and its resilience to other interferers from the perspective of electrode utilization. Based on the research, an equivalent reference distance is developed to determine the proper electrode size for the required body channel characteristics and to gain an engineering insight on BCC.

This paper is organized as follows. Section II introduces nine kinds of electrode configurations according to the arrangement

Manuscript received July 22, 2014; revised November 14, 2014 and January 14, 2015; accepted February 06, 2015. Date of publication February 20, 2015; date of current version April 02, 2015. This work was supported by the National Research Foundation of Korea (NRF) funded by the Ministry of Science, ICT and Future Planning under the Basic Science Research Program (NRF-2012R1A2A1A01008937).

The authors are with the Department of Electrical Engineering, Korea Advanced Institute of Science and Technology (KAIST), Daejeon 305-701, Korea (e-mail: joonsung.bae@kaist.ac.kr; hjyoo@kaist.ac.kr).

Color versions of one or more of the figures in this paper are available online at <http://ieeexplore.ieee.org>.

Digital Object Identifier 10.1109/TMTT.2015.2402653

and direction of electrodes on the body, and the configurations are modeled by means of vertical and horizontal electric dipoles. Section III gives the complete equations of the vertical and horizontal electric fields on the human body to theoretically address the body channel characteristics and the effects of electrode configurations on BCC. The measurement setup and results to verify the theory are then shown in Section IV. In addition, the influence of BCC and RF interference on the body channel is investigated and discussed along with receiving electrode configurations for the purpose of proper electrode utilization in the design of BCC systems. Based on the theoretical study and the measurement results, Section V provides the frequency response model of BCC to determine the proper electrode size in the design of BCC systems. Finally, Section VI concludes this paper.

II. ELECTRODE CONFIGURATIONS FOR BCC

BCC utilizes electrodes attached to the human body in order to transmit and receive electrical signals as a communication interface between the body and the BCC TRX. In general, a signal electrode and a GND electrode are required in both sides of the transmitter (TX) and receiver (RX) to constitute the electrical forward and return path while the potential difference generated by the TX is differentially sensed by the RX. From the perspective of electrode utilization, only a signal electrode can be attached to the human body while the other GND electrode is floated or is not in contact with the body. Otherwise, two electrodes are attached to the body in the longitudinal or transversal direction. Fig. 1 depicts a diagram of the respective electrode configurations in the TX and RX, which can be exploited in BCC. In this paper, we can express the cases of one electrode contact in Fig. 1(a), two electrodes contact in the longitudinal direction in Fig. 1(b), and transversal direction in Fig. 1(c) in a vertical, horizontal (0°), and horizontal (90°) configuration, respectively. As a result, the theoretical analysis in the previous research [10] that assumed only vertical electrodes can be expanded by incorporating the cases of the horizontal electrodes to understand the effects of electrode configurations on BCC.

Since BCC is based upon the principle of electric field propagation from dipole sources [10], Fig. 2 shows the simplified description of BCC by means of the electric field from dipole sources to obtain the electric field intensity above that of the human body. In the TX side, the vertical and horizontal electrodes in Fig. 1 are modeled by vertical dipole [E^v in Fig. 2(a)], horizontal dipole with longitudinal direction [E^{h0} in Fig. 2(b)], and horizontal dipole with transversal direction [E^{h90} in Fig. 2(c)]. In the case of the RX electrode configuration, we can detect the electric field intensity at the distance of r from the dipole source with vertical, horizontal (0°), and horizontal (90°) electrodes. The vertical, horizontal (0°), and horizontal (90°) electrodes can sense the E_r component, E_ϕ component, and E_z component, respectively. Therefore, as shown in Fig. 3, three kinds of electrode configurations in both the TX and RX introduce nine TRX configurations that can be quantified by electric field intensity. For instance, E_z^v in the case of 1-1 indicates the electric field intensity of the z -component away from vertical dipole source, which models the case in which

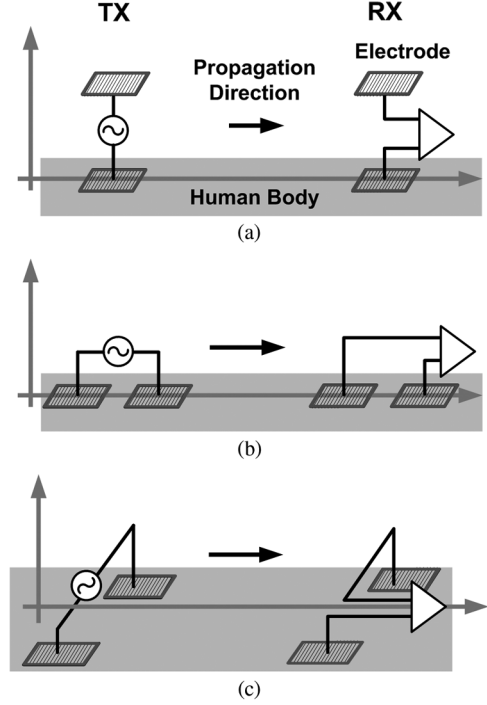


Fig. 1. Electrode configurations. (a) Vertical electrodes. (b) Horizontal electrodes with longitudinal direction. (c) Horizontal electrodes with transversal direction.

vertical electrodes in the TX and vertical electrodes in the RX are employed.

III. THEORETICAL ANALYSIS

A. Electric Field From Vertical and Horizontal Dipoles

Assuming the surface of the human body is an infinite half-plane with a finite conductivity (σ) and permittivity (ϵ), as shown in Fig. 2, we calculate the electric field intensity of the r -, ϕ -, and z -directions at the distance of r from the vertical and horizontal dipole sources. From Maxwell's equations, the vertical and horizontal electric field intensities from the vertical and horizontal dipole sources are given by Norton in [12] and [13], which describe the general equations of electric fields at any point above the surface. Given that the electrodes are near the surface of the human body for BCC applications, we can suppose the dipole sources are located at $z = 0$, and electric fields are calculated at $z = 0$, as shown in Fig. 2. Consequently, the equations of the electric field intensity corresponding to the nine cases described in Fig. 3 can be derived and simplified as follows.

Case 1-1

$$E_z^v = 2ik \left[(1 - u^2 + u^4)F - \frac{1}{ikr} + \frac{1}{(ikr)^2} \right] \frac{e^{i(kr - \omega t)}}{r}. \quad (1)$$

Case 1-2

$$E_r^v = ik \left[u\sqrt{1 - u^2}(2 - u^2 + u^4)F - u\sqrt{1 - u^2}(1 + F) \right. \\ \left. \cdot \frac{1}{ikr} + 0 \cdot \frac{1}{(ikr)^2} \right] \frac{e^{i(kr - \omega t)}}{r}. \quad (2)$$

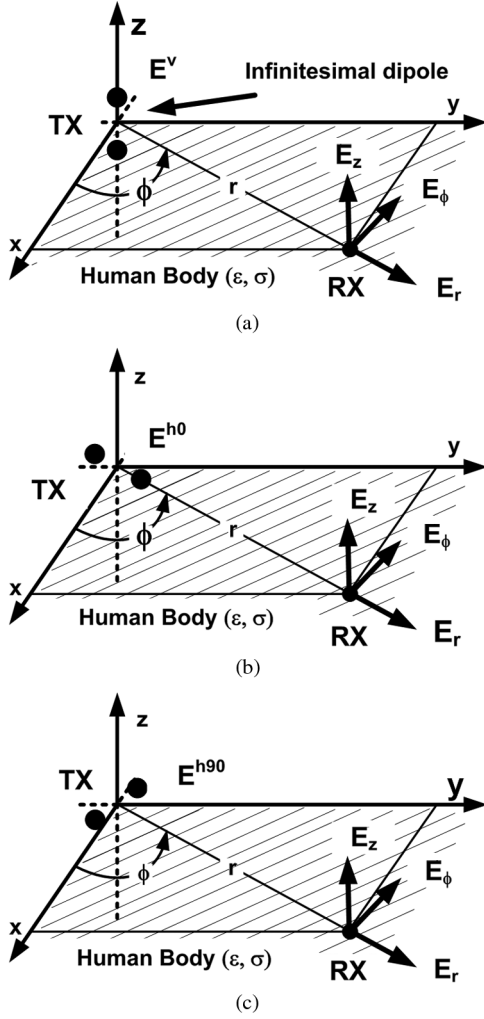


Fig. 2. Electric field from dipole sources. (a) Vertical dipole. (b) Horizontal dipole with longitudinal direction. (c) Horizontal dipole with transversal direction.

	Vertical RX	Horizontal (0°) RX	Horizontal (90°) RX
Vertical TX	Case 1-1 E_z^v 	Case 1-2 E_r^v 	Case 1-3 E_ϕ^v
Horizontal (0°) TX	Case 2-1 E_z^{h0} 	Case 2-2 E_r^{h0} 	Case 2-3 E_ϕ^{h0}
Horizontal (90°) TX	Case 3-1 E_z^{h90} 	Case 3-2 E_r^{h90} 	Case 3-3 E_ϕ^{h90}

Fig. 3. Nine types of electrode configuration in BCC.

Case 1-3

$$E_\phi^v = 0. \quad (3)$$

Case 2-1

$$E_z^{h0} = ik \left[u \sqrt{1-u^2} (2-u^2+u^4) F - u \sqrt{1-u^2} (1+F) \cdot \frac{1}{ikr} + 0 \cdot \frac{1}{(ikr)^2} \right] \frac{e^{i(kr-\omega t)}}{r}. \quad (4)$$

Case 2-2

$$E_r^{h0} = 2ik \left[u^2 (1-u^2+u^4) F - G - u^2 [1 + (1-u^2+u^4) F] \cdot \frac{1}{ikr} + u^2 (1+F) \cdot \frac{1}{(ikr)^2} \right] \frac{e^{i(kr-\omega t)}}{r}. \quad (5)$$

Case 2-3

$$E_\phi^{h0} = 0. \quad (6)$$

Case 3-1

$$E_z^{h90} = 0. \quad (7)$$

Case 3-2

$$E_r^{h90} = 0. \quad (8)$$

Case 3-3

$$E_\phi^{h90} = ik \left[2G - u^2 (2-u^2+u^4) F \cdot \frac{1}{ikr} + u^2 (1+F) \cdot \frac{1}{(ikr)^2} \right] \frac{e^{i(kr-\omega t)}}{r} \quad (9)$$

$$u = 1/\sqrt{(\epsilon + ix)} \quad (10)$$

$$\text{erfc}(x) = \frac{2}{\pi} \int_x^\infty e^{-u^2} du \quad (11)$$

$$F = [1 + i\sqrt{\pi p_1} e^{-p_1} \text{erfc}(-i\sqrt{p_1})] \quad (12)$$

$$p_1 = ikr(1-u^2)u^2/2 \quad (13)$$

$$G = [1 + i\sqrt{\pi q_1} e^{-q_1} \text{erfc}(-i\sqrt{q_1})] \quad (14)$$

$$q_1 = ikr(1-u^2)/2u^2 \quad (15)$$

where r is the distance from the dipole source, the wavenumber is $k = 2\pi/\lambda$, the relative conductivity is $x = 1.8 \cdot 10^{10} \cdot \sigma_{\text{emu}}/f$ or $\sigma_{\text{emu}}/(2\pi\epsilon_0)$, ϵ is the dielectric constant of the human body referring to air as unity while σ_{emu} is the conductivity of the human body in electromagnetic unit, f is the operating frequency, and λ is the corresponding wavelength. In addition, $\text{erfc}(x)$ denotes error function, F is a vertical attenuation function, and G is a horizontal attenuation function. One electromagnetic unit of conductivity is 10^{11} S/m because the resistivity ρ of $1 \Omega \cdot \text{m}$ in the International System of Units (SI unit) corresponds to the resistivity of $(10^{11}) \text{ ab}\Omega \cdot \text{cm}$ in electromagnetic units.

The intensities of the electric fields described in (1)–(9) are a function of the communication distance and the wavenumber and can be generally expressed in the following form with respect to variables r and k :

$$E(r, k) = i \left(A \cdot k \cdot \frac{1}{r} + i \cdot B \cdot \frac{1}{r^2} - C \cdot \frac{1}{k} \frac{1}{r^3} \right) e^{i(kr-\omega t)} \quad (16)$$

where A , B , and C are coefficients composed of a complex permittivity (u) of (10), a vertical attenuation factor (F) of (12), and a horizontal attenuation factor (G) of (14) at a given r and

TABLE I
EXPRESSIONS FOR A , B , AND C IN EACH ELECTRODE CONFIGURATION CASE

	A	B	C
Case 1-1 (E_z^v)	$2(1 - u^2 + u^4)F$	2	2
Case 1-2 (E_r^v)	$u\sqrt{1 - u^2}(2 - u^2 + u^4)F$	$u\sqrt{1 - u^2}(1 + F)$	0
Case 1-3 (E_ϕ^v)	0	0	0
Case 2-1 (E_z^{h0})	$u\sqrt{1 - u^2}(2 - u^2 + u^4)F$	$u\sqrt{1 - u^2}(1 + F)$	0
Case 2-2 (E_r^{h0})	$2(u^2(1 - u^2 + u^4)F - G)$	$2u^2(1 + (1 - u^2 + u^4)F)$	$2u^2(1 + F)$
Case 2-3 (E_ϕ^{h0})	0	0	0
Case 3-1 (E_z^{h90})	0	0	0
Case 3-2 (E_r^{h90})	0	0	0
Case 3-3 (E_ϕ^{h90})	$2G$	$u^2(2 - u^2 + u^4)F$	$u^2(1 + F)$

k , which are listed in Table I with respect to each case. The complex permittivity (u) includes the characteristics of the human body while the vertical (F) and horizontal (G) attenuation factors represent an inherent property of electric fields at the surface of the half-plane with finite conductivity and permittivity. Equation (16) consists of three terms, which are the term proportional to k with the first order in $1/r$, the term with $1/r^2$, and the term inversely proportional to k with $1/r^3$. In general, $1/r$, $1/r^2$, and $1/r^3$ terms correspond to the dominant electric field in the far-field, induction-field, and near-field of the dipole, respectively. The far-field propagation term has a significant effect on the electric field intensity as the wavenumber k , which is proportional to the operating frequency, increases, whereas the quasi-static coupling term is negligible. Therefore, when the kr , wavenumber times distance, decreases, the near-field third term in (16) is dominant compared to the other terms, while when the kr increases, the far-field first term in (16) becomes the principal term.

Lastly, as shown in Table I, it should be noted that: 1) the electric field intensities in Case 1-3, Case 2-3, Case 3-1, and Case 3-2 are theoretically zero since the direction of the dipole source and receiving component are orthogonal and, therefore, uncorrelated; 2) the electric field intensities in Case 1-2 and Case 2-1 are identical; and 3) the values of C in the Case 1-2 and Case 2-1 are zero, and the electric field intensities do not contain any near-field component, which means the received signal using electrode configurations of Cases 1-2 and 2-1 is not affected by the near-field term.

B. Channel Characteristics of BCC

The electric field intensities derived in (1)–(9) are a function of the channel distance and the frequency. Furthermore, based on the equations, we can quantify the channel response or transfer function of BCC, which is expressed as the magnitude ratio of the received electric field intensity to the transmitted electric field intensity. To set up the frequency response of BCC, Fig. 4 depicts the situation modeling the intensity of the transmitted electric field (E_{TX}) and received electric field (E_{RX}). The E_{RX} can be simply described by means of the electric field intensity at the distance r from the TX (dipole source), such as $E_{\text{receiving direction}(z,r,\phi)}^v(r)$ with the vertical TX in Fig. 4(a), $E_{\text{receiving direction}(z,r,\phi)}^{h0}(r)$ with horizontal(0°) TX in Fig. 4(b), and $E_{\text{receiving direction}(z,r,\phi)}^{h90}(r)$ with horizontal(90°) TX in Fig. 4(c). On the other hand, the expressions

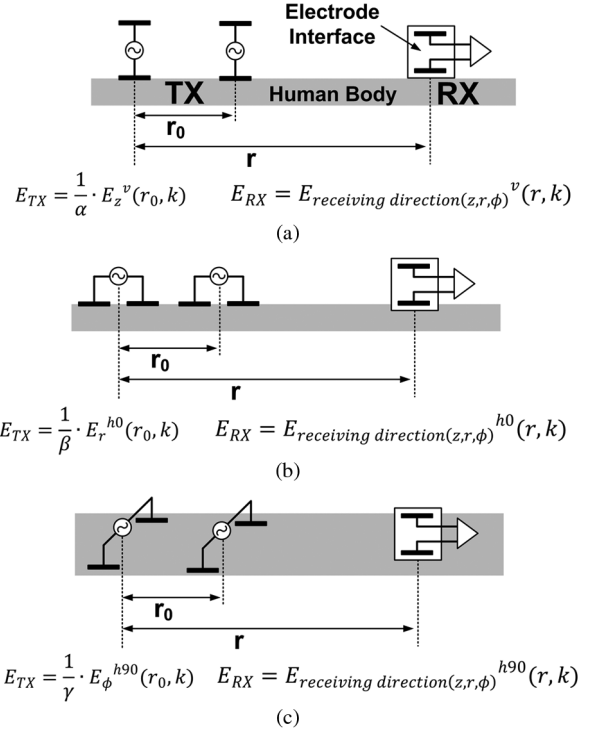


Fig. 4. Electric field intensity in TX and RX. (a) Vertical source. (b) Horizontal source with longitudinal direction. (c) Horizontal source with transversal direction.

for E_{TX} should take account of the finite physical size of the electrode since when the transmitted electric field is calculated at the distance r of 0, it goes to infinite value. Therefore, we can assume the reference distance r_0 , regarded as the transmitting point to quantify the transmitted electric field intensity (E_{TX}) by taking advantage of the electric field intensity at the distance r_0 . When the attenuation constants α , β , and γ are defined as the ratio of the electric field intensity at the distance r_0 with the vertical TX of Fig. 4(a), horizontal (0°) TX of Fig. 4(b), and horizontal (90°) TX of Fig. 4(c) to the transmitted electric field intensity (E_{TX}), respectively, in each electrode case, we can write

$$|E_{TX}| = \frac{1}{\alpha} \cdot |E_z^v(r_0)| = \frac{1}{\beta} \cdot |E_r^{h0}(r_0)| = \frac{1}{\gamma} \cdot |E_\phi^{h90}(r_0)| \quad (17)$$

TABLE II
EXPRESSIONS FOR FREQUENCY RESPONSE IN EACH ELECTRODE
CONFIGURATION CASE

TX \ RX	Vertical	Horizontal (0°)	Horizontal (90°)
Vertical	$\frac{E_z^v(r, k)}{E_z^v(r_0, k)}$	$\frac{E_r^v(r, k)}{E_z^v(r_0, k)}$	$\frac{E_\phi^v(r, k)}{E_z^v(r_0, k)}$
Horizontal (0°)	$\frac{E_z^{h0}(r, k)}{E_z^v(r_0, k)}$	$\frac{E_r^{h0}(r, k)}{E_z^v(r_0, k)}$	$\frac{E_\phi^{h0}(r, k)}{E_z^v(r_0, k)}$
Horizontal (90°)	$\frac{E_z^{h90}(r, k)}{E_z^v(r_0, k)}$	$\frac{E_r^{h90}(r, k)}{E_z^v(r_0, k)}$	$\frac{E_\phi^{h90}(r, k)}{E_z^v(r_0, k)}$

Thus, the frequency responses of BCC with respect to the TX electrode configurations are obtained as follows:

$$|H^v(r, k)| = \left| \frac{E_{RX}}{E_{TX}} \right| = \left| \frac{E_{RX \text{ direction}(z, r, \phi)}^v(r, k)}{E_z^v(r_0, k)} \cdot \alpha \right| \quad (18)$$

$$|H^{h0}(r, k)| = \left| \frac{E_{RX}}{E_{TX}} \right| = \left| \frac{E_{RX \text{ direction}(z, r, \phi)}^{h0}(r, k)}{E_r^{h0}(r_0, k)} \cdot \beta \right| = \left| \frac{E_{RX \text{ direction}(z, r, \phi)}^{h0}(r, k)}{E_r^{h0}(r_0, k)} \cdot \frac{E_r^{h0}(r_0, k)}{E_z^v(r_0, k)} \cdot \alpha \right| = \left| \frac{E_{RX \text{ direction}(z, r, \phi)}^{h0}(r, k)}{E_z^v(r_0, k)} \cdot \alpha \right| \quad (19)$$

$$|H^{h90}(r, k)| = \left| \frac{E_{RX}}{E_{TX}} \right| = \left| \frac{E_{RX \text{ direction}(z, r, \phi)}^{h90}(r, k)}{E_\phi^{h90}(r_0, k)} \cdot \gamma \right| = \left| \frac{E_{RX \text{ direction}(z, r, \phi)}^{h90}(r, k)}{E_\phi^{h90}(r_0, k)} \cdot \frac{E_r^{h90}(r_0, k)}{E_z^v(r_0, k)} \cdot \alpha \right| = \left| \frac{E_{RX \text{ direction}(z, r, \phi)}^{h90}(r, k)}{E_z^v(r_0, k)} \cdot \alpha \right| \quad (20)$$

For simplicity, we assume the attenuation constant α is unity to calculate and compare each transfer function H^v , H^{h0} , and H^{h90} in (18)–(20), respectively, which is summarized with all configuration cases in Table II. It is noteworthy that the transfer function is expressed with the ratio of the received electric field at the distance r to the electric field of E_z^v in (1) at the reference distance of r_0 . Finally, the transfer function of BCC is given by

$$\frac{|E_{RX}(r, k)|}{|E_z^v(r_0, k)|} = \frac{|A \cdot k \cdot \frac{1}{r} + i \cdot B \cdot \frac{1}{r^2} - C \cdot \frac{1}{k} \cdot \frac{1}{r^3}|}{2 \cdot |(1 - u^2 + u^4)F(r_0, k) \cdot k \cdot \frac{1}{r_0} + i \cdot \frac{1}{r_0^2} - \frac{1}{k} \cdot \frac{1}{r_0^3}|} \quad (21)$$

where r is the communication distance, k is the wavenumber of the operating frequency, r_0 is the reference distance, and A , B , and C are in Table I.

As mentioned before, since the first term of (16) is proportional to the frequency, and the third term of (16) is inversely proportional to the frequency, in a high-frequency range the first term of (16) is dominant over the third term of (16) and *vice versa* at the low frequency. Therefore, the frequency response could be simplified in accordance with the frequency range as the following equation:

$$\frac{|E_{RX}(r, k)|}{|E_z^v(r_0, k)|} = \begin{cases} \left| \frac{C}{2} \cdot \frac{r_0^3}{r^3} \right|, & \text{at a low frequency} \\ \left| \frac{A}{2(1 - u^2 + u^4)F(r_0, k)} \cdot \frac{r_0}{r} \right|, & \text{at a high frequency.} \end{cases} \quad (22)$$

In the low-frequency domain, the frequency response is affected by the value of C and $(r_0/r)^3$, whereas, at the high-frequency range, the values of A and (r_0/r) have an effect on the frequency response. To obtain qualitative analysis of the body channel response, the numerical values of A , B , and C in Table I are given as a function of frequency in Fig. 5 by using conductivity and dielectric properties of human dry skin [14] when r is fixed to 1 m. According to Fig. 5 and (22), C and (r_0/r) is smaller than A and 1, respectively; therefore, $C \cdot (r_0/r)^3$ is far smaller than $A \cdot (r_0/r)$. As the frequency increases, the magnitude of the response increases. As a result, the frequency response has the appearance of high-pass characteristics at a low-frequency region. In addition, because the value of A decreases at a high-frequency region, the magnitude of the response decreases as the frequency increases, which means, in general, the frequency responses in BCC look like bandpass characteristics, regardless of the electrode configuration.

To concentrate on the effect of each electrode configuration on the channel, we can compare the magnitude of the frequency response in each electrode case as shown in Fig. 6. The graphs of decibel scaled transmission gain are plotted with the values obtained from the numerical analysis in Fig. 6 with respect to the log-scaled frequency range from 100 kHz to 1 GHz when r and r_0 are set to 2 and 0.3 m in Fig. 6(a), 1 and 0.3 m in Fig. 6(b), and 2 and 0.1 m in Fig. 6(c), respectively. We omit the cases in 1-3, 2-3, 3-1, and 3-2 because the magnitude of the responses is theoretically equal to zero. Case 2-1 is not shown in the graph either since the frequency response of Case 2-1 is the same as that of Case 1-2. We can confirm that Fig. 6 shows the bandpass channel characteristics of BCC. Since Cases 1-1 and 1-2 show a higher transmission gain than Cases 2-2 and 3-3, the path loss of the vertical electrode configuration with one electrode in contact has an advantage over the horizontal electrode configuration with two electrodes in contact. Moreover, Fig. 6 shows the following: 1) the low-frequency channel response in Case 1-1 is mainly determined by channel distance (r_0/r) due to the constant value of C ($= 2$), while the effect of channel distance is negligible in Cases 1-2, 2-2, and 3-3 since the value of C is nearly 0 and far smaller than the value in Case 1-1 and 2) the high-frequency channel response in Case 3-3 is in rapid decline compared to the other cases because the value of A in Case 3-3

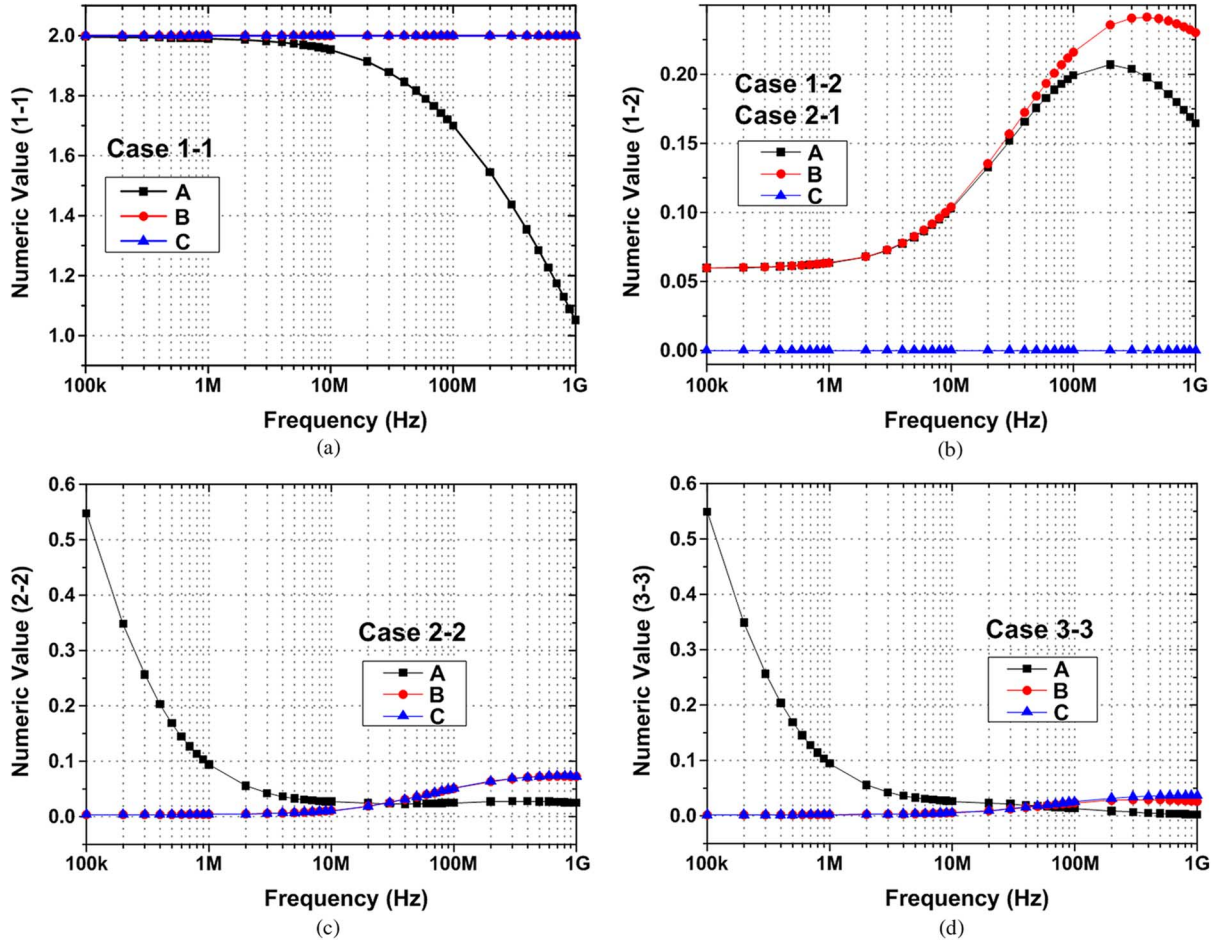


Fig. 5. Numerical values of A , B , and C in each case. (a) Case 1-1. (b) Case 1-2. (c) Case 2-2. (d) Case 3-3.

represents the highest attenuation rate in the high frequency region. Therefore, it should be noted that Case 1-1 shows superior transmission gain, but it is susceptible to the surrounding environment. Finally, the magnitude of the frequency response of the body channel declines with the large r [see Fig. 6(d)] and the small r_0 , and its bandwidth is lowered with the large r_0 , which implies that: 1) the transmission gain is lowered with a long channel distance and 2) the transmission gain decreases and channel bandwidth increases when we set the small reference distance (r_0) in the numerical analysis.

IV. BODY CHANNEL MEASUREMENT

A. Measurement Setup

The frequency response of the body channel is performed to verify the theoretical analysis with respect to the electrode configurations. The main purpose of the measurement is to compare the frequency response with different electrode configurations. Therefore, we employ a balun transformer [7] with a network analyzer for simplicity, as presented in Fig. 7(a). However, since parasitic coupling capacitance exists between the primary and secondary coils in the balun, described as $C_{\text{parasitic}}$ in Fig. 7(a), the common-mode signal may flow through the balun and prevent accurate measurement of BCC [16]. Nevertheless,

the balun can conveniently separate the TX and RX from each other and the effect of the external GND.

The output power of the TX side in the network analyzer is set to 0 dBm, which corresponds to the V_{rms} value (square root of the mean of the square (rms) value of the voltage for one time period of the ac sine wave) of 0.22 V and I_{rms} value (rms value of the ac current) of 4.4 mA when the 50- Ω matched network analyzer is exploited to measure the channel response. The I_{rms} value of 4.4 mA is far less than the 40 mA, which is the maximum occupational exposure guideline value from the International Commission on Non-Ionizing Radiation Protection (INIRP). The network analyzer is connected with commercial FTB-1-6 baluns at the RX and TX side, and the interface between the human body and the balun is through circular 3M Red Dot electrodes in order to make a secure contact to the human body and minimize the effect of the motion artifact. The two electrodes, which constitute the vertical or horizontal dipole are linked to differential inputs of the balun via the small printed circuit board (PCB) with an SMA interface. For the horizontal configuration, two 3M Red Dot electrodes are in contact with the body. On the other hand, for the vertical configuration, only one 3M Red Dot electrode is in contact with the body and GND port is floated. Therefore, the GND electrode in the vertical configuration is made by the GND plane of the PCB interface board. The distance between the signal and GND electrodes in horizontal

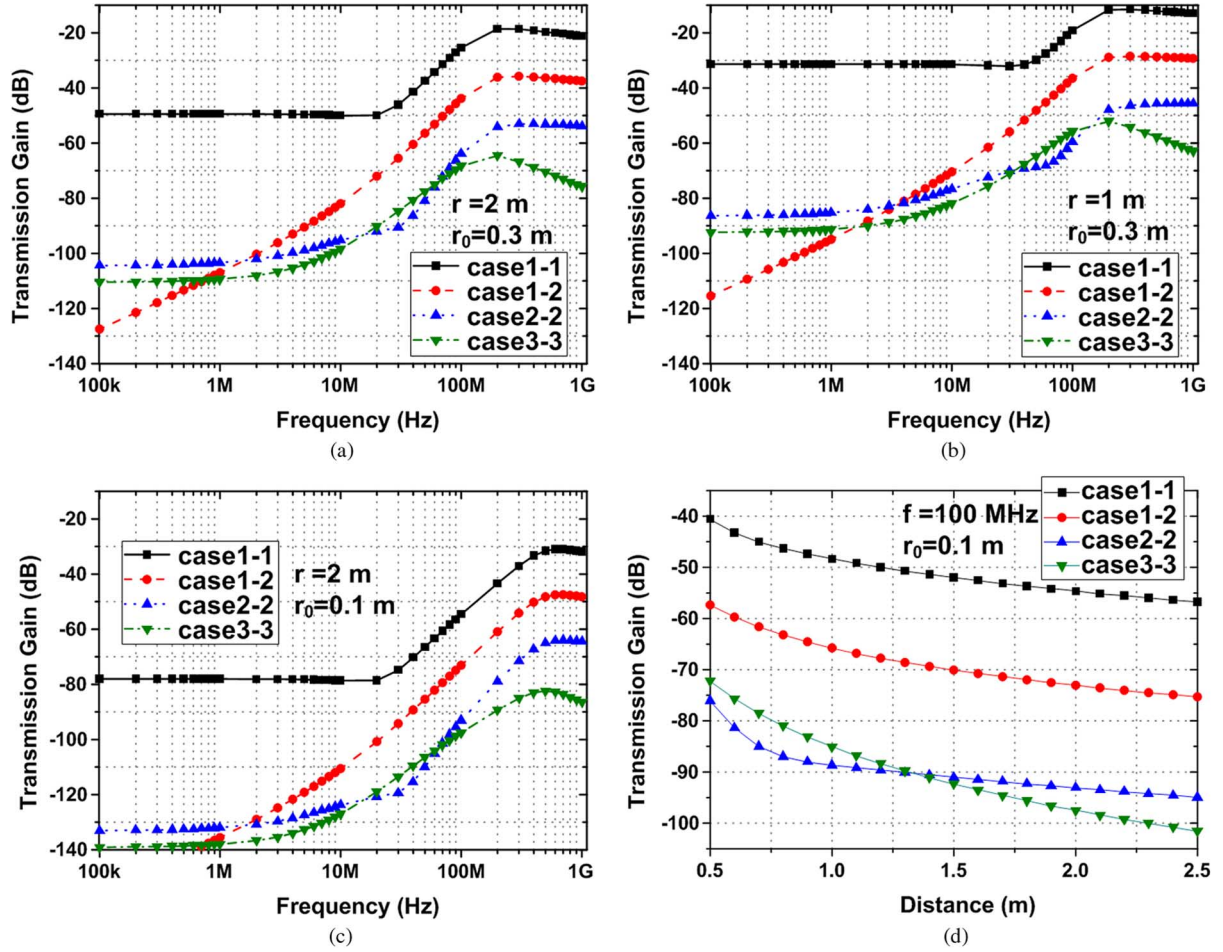


Fig. 6. Frequency response using theoretical analysis. (a) When $r = 2$ m, $r_0 = 0.3$ m. (b) When $r = 1$ m, $r_0 = 0.3$ m. (c) When $r = 2$ m, $r_0 = 0.1$ m. (d) Effect of r when $f = 100$ MHz and $r_0 = 0.1$ m.

configurations is 3, 4, and 5 cm for the electrode's diameters of 3, 4, and 5 cm, respectively, as shown in the image of the measurement setup [the bottom of Fig. 7(a)].

The height of the human subject is 1.9 m, and the RX and TX electrodes are attached to the human body isolated from the external ground by more than 0.9 m, and we utilize three kinds of circular electrodes, which have diameters of 3, 4, and 5 cm. The output of the balun is applied to the network analyzer through 50 Ω —match shielded coaxial cable. We try to prevent utilizing long cable to reduce the antenna and coupling effect of the cable. The parasitic components from the balun and cables are adequately eliminated by connecting them to a network analyzer during the calibration process before the measurement. The frequency response is measured in the frequency range from 1 to 100 MHz and at the channel distance between the TX and RX from 0.5 to 1 m. In addition to the channel characteristics, the influence of the BCC interference coming from vertical and horizontal electrode configurations and RF interference from the FM antenna on BCC is further investigated along with three receiving electrode configurations. Fig. 7(b) shows the measurement setup for the interferers. We inject the interference signal of BCC with vertical and horizontal electrode configuration, and the interference signal of the RF through the FM antenna. The battery-powered board with an 80-MHz crystal oscillator is utilized as an interferer. Both the BCC and RF interferer are 1 m

away from the RX, and the output power is set to 0 dBm. A spectrum analyzer with a balun as the RX measures the power of the received signal power from the interferers with respect to the RX electrode configurations.

B. Channel Characteristics of BCC

The channel characteristics of BCC, which is S_{21} -parameters of the network analyzer through the coaxial cable, balun, electrode, and body channel, are measured with respect to the electrode configurations. Fig. 8 shows the measured frequency responses of BCC in decibels with a channel distance (r) of 0.5 m with an electrode diameter (ϕ) of 4 cm in Fig. 8(a), a channel distance of 1 m with an electrode diameter of 4 cm in Fig. 8(b), and a channel distance of 0.5 m with an electrode diameter of 3 cm in Fig. 8(c). As we observed in the theoretical analysis results, the magnitude of the frequency responses in Cases 1-3, 2-3, 3-1, and 3-2 result in lower value, and the frequency response in Case 2-1 is similar with that of Case 1-2. Therefore, for simplicity, Case 1-1, Case 1-2, Case 2-2, and Case 3-3 are only considered in Fig. 8 like the case of Fig. 6. At a low frequency, the body channel has high-pass characteristics with a slope of 20 dB/dec regardless of the channel distance, electrode diameter, and electrode configuration since the electric field is relatively constant across the entire human body due

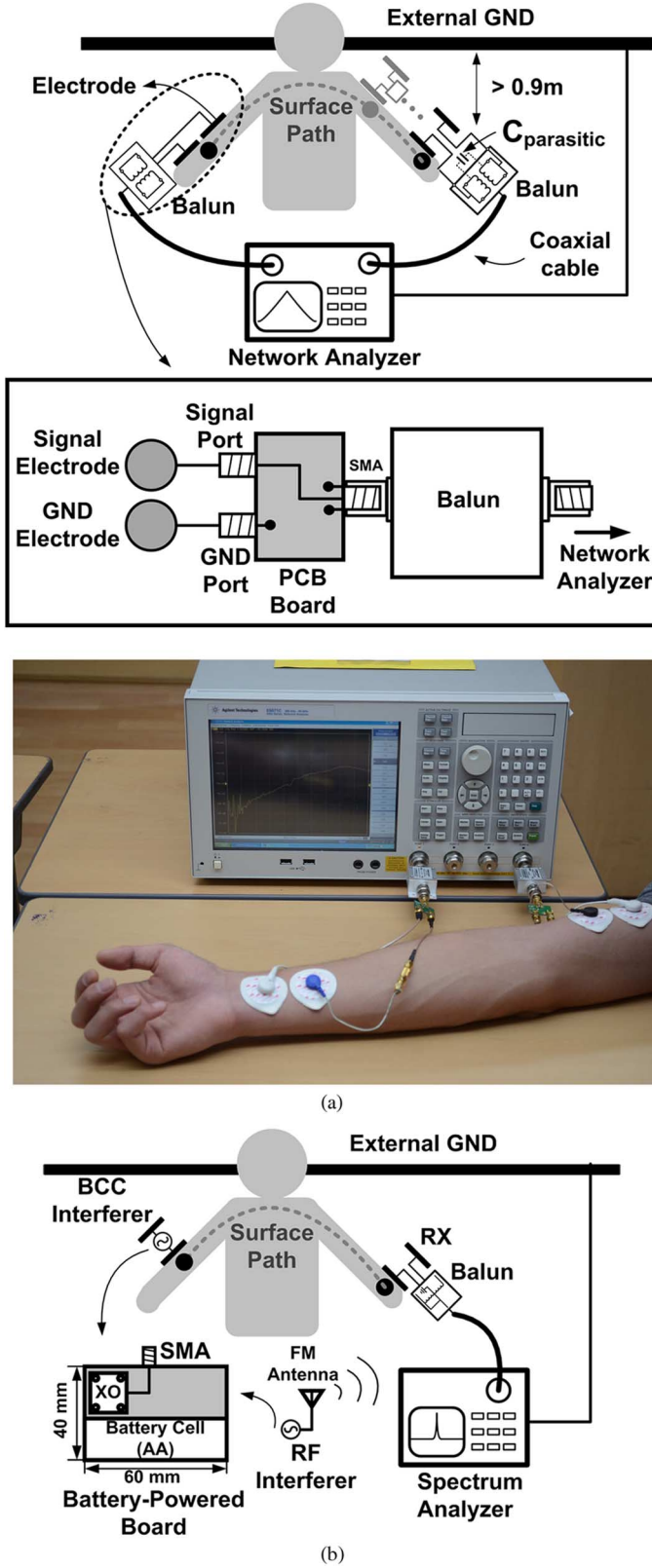


Fig. 7. Measurement setup. (a) Frequency response. (b) Interferers.

to the near-field coupling mechanism at low frequency. However, the channel distance greatly influences the frequency response beyond 50 MHz, as shown in Fig. 8(d). The attenuation slopes in Cases 1-1, 1-2, 2-2, and 3-3 are almost linear with

a bit different slope, which means the signal attenuates exponentially with channel length because the far-field propagation mechanism starts to have an effect on the channel characteristics [10]. As the frequency and the distance increase, the far-field signal is attenuated more and induces larger signal loss. As a result, the frequency response goes gradually down and its bandwidth decreases with the distance. When compared to Fig. 8(a), Fig. 8(c) shows the effect of the electrode size. While the small electrode size makes the magnitude of the response decrease, it increases the cutoff frequency and bandwidth of the channel. As discussed in Section III-B, it is noted that the effect of the electrode size is similar to that of the reference distance r_0 .

When it comes to the comparison of the effects of the electrode configurations on BCC, the transmission gain is unconditionally superior in Case 1-1. The usage of the vertical electrodes guarantees the high magnitude of the frequency response, regardless of whether they are adopted in the TX (Case 1-2), RX (Case 2-1), or both (Case 1-1). However, during the measurement, it is found that the floated electrode in the vertical configuration is susceptible to the surrounding environment, such as the external GND, and movement of the body and cables. This is because in the vertical electrodes, the signal return path passes through the environment around the body. Consequently, although the magnitude of the frequency response is not better than the vertical electrode configuration, the horizontal electrode configuration is robust to the surrounding environment. In conclusion, the measurement result agrees fairly well with the theoretical frequency response of Fig. 6 in terms of the transmission gain (E_{RX}/E_{TX}), channel distance (r), and reference distance (r_0) provided that we can derive the correlation between the reference distance (r_0) and the electrode diameter (ϕ).

C. Path Loss Characteristics in the 21-MHz Human Body Communication (HBC) Band

The frequency band of the HBC of IEEE 802.15.6 [3] is centered at 21 MHz with 5.25 MHz. Therefore, it is useful to discuss the body channel characteristics around 21 MHz with respect to the electrode configurations. As shown in Fig. 8, at the frequency of 21 MHz, the frequency response looks like a high-pass filter, which means the signal propagation is mainly determined by the capacitive impedance. Therefore, in the HBC band, the near-field quasi-static mechanism prevails over the far-field surface wave mechanism, and that is why we also call the HBC near-field capacitive coupling communication [10].

Furthermore, to provide practical insight into the channel characteristics in the HBC band, the path-loss characteristics for on-body transmission are formulated based on the measurement results in Fig. 8. The path-loss characteristics in the 21-MHz band can be expressed by

$$PL \begin{cases} PL_0, & d = 0.5 \\ PL_0 + \alpha_0(d - 0.5), & d > 0.5 \end{cases} \quad (23)$$

where PL is the path loss in units of dB, α_0 is the path loss per unit distance in units of dB/m in the near-field region, d is the channel distance, and PL_0 is the path loss at the channel distance of 0.5 m. The PL_0 is given, and then α_0 can be obtained from the linear fitting by the measurement results. Table III summarizes the list of PL_0 and α_0 at a frequency of 21 MHz in the case

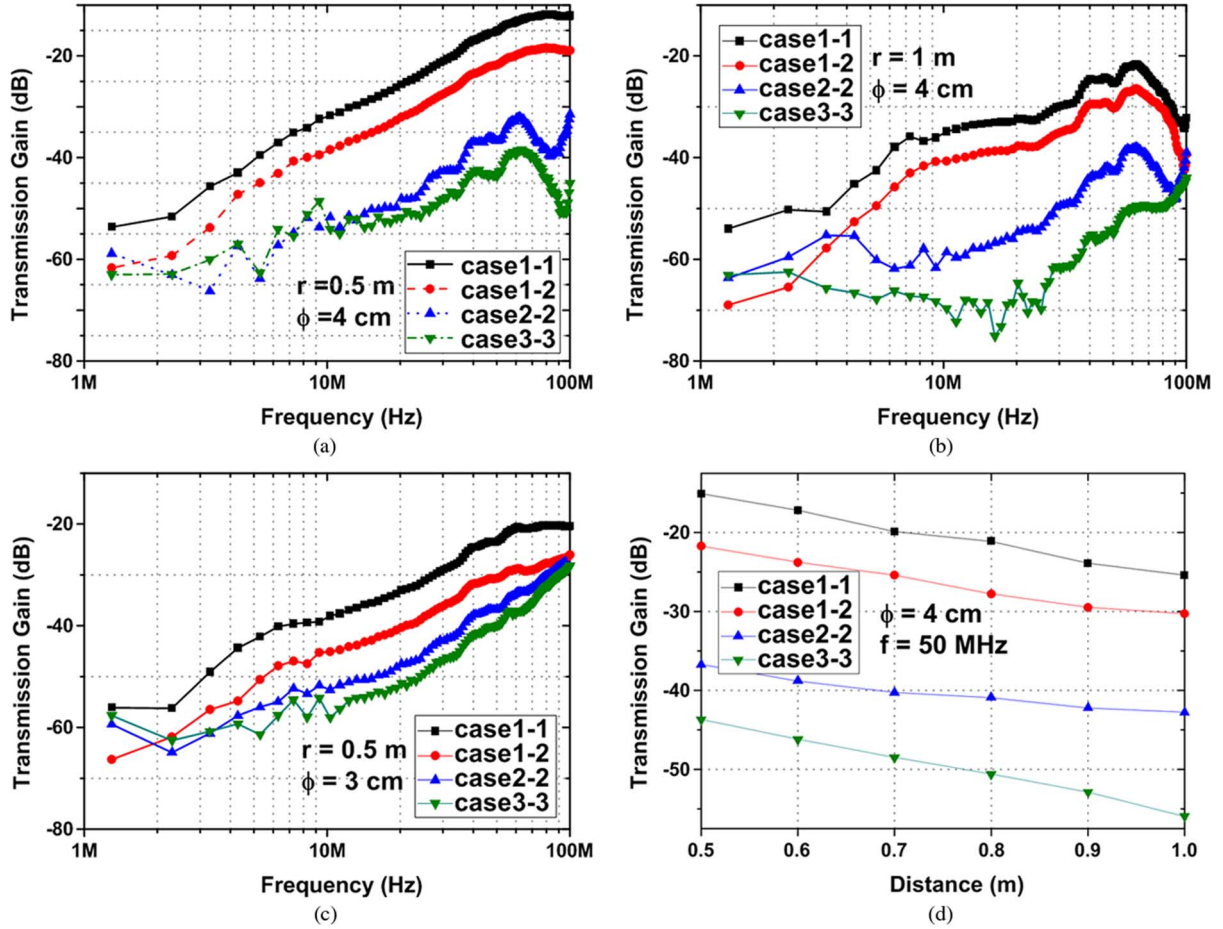


Fig. 8. Measured frequency response: (a) with a distance of 0.5 m and electrode diameter of 4 cm, (b) with a distance of 1 m and diameter of 4 cm, (c) and with a distance of 0.5 m and diameter of 3 cm. (d) Effect of the distance when $f = 50$ MHz, diameter of 4 cm.

of 1-1, 1-2, 2-2, and 3-3. It is noted that the path loss per unit distance is severe in the case of 3-3, compared to the other cases.

D. Electrode Configurations and Interference

Since the RX senses all signals through the human body, the unwanted interference signal affects the signal-to-noise ratio of the received signal. It is possible to properly attenuate if we actively utilize the property of the electrode configuration in the RX. There are two possible interferers through the body. One is interference from other BCC devices in case of multi-channel communication. When the TX source in Fig. 3 is regarded as the BCC interferer, the effect of the BCC interferer with vertical and horizontal electrodes on the various RX configurations can also be obtained by Table II. On the contrary to the transmission gain, when the interferer and RX constitute the electrode configurations of Case 1-3, Case 2-3, Case 3-1, and Case 3-2, the RX shows better resilience to the interferer. From the measurement setup of Fig. 7(b), the measured RX signal powers in Case 1-1, Case 1-2, Case 2-2, and Case 3-3 are -27.2 , -30.5 , -39.1 , and -44.7 dBm, respectively. As expected, Case 1-1, which means the interferer with vertical electrodes into the RX with vertical electrodes, is the most vulnerable combination.

On the other hand, another interferer is the signal induced by the RF source outside of the human body due to the body antenna effect [15]. The human body under electromagnetic fields

TABLE III
PARAMETERS OF PATH LOSS @ 21 MHz

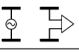
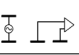
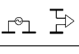
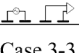
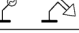
Electrode Configuration	α_0 [dB/m]	PL_0 [dB]
Case 1-1	14.44	25.17
Case 1-2	12.18	31.66
Case 2-2	12.34	48.18
Case 3-3	28.12	50.63

behaves as a wideband antenna in the 40–400-MHz frequency range since its resonance frequency is determined by a wavelength equal to twice the average human height. The measured RX signal powers via the vertical, horizontal (0°), and horizontal (90°) electrodes are -28.7 , -36.9 , and -36.6 dBm, respectively, which indicates that the horizontal RX electrodes are a better option than the vertical RX electrodes to mitigate the body antenna effect.

Based on the theoretical analysis and the measurement results, Table IV summarizes the characteristics of the TRX electrode configurations in regard to the transmission gain, environmental sensitivity, and interference resilience for the purpose of electrode utilization in the design of BCC systems. Taking account of the overall aspect, since there is no inferior performance item in Case 1-2, the TRX electrode configuration of the

TABLE IV
COMPARISON AND SUMMARY OF ELECTRODE CONFIGURATION

●: Good ▲: Normal ✕: Poor

	Trans. Gain	Robust to Environm.	Resilience to Interference			
			BCC			RF
			Vertic.	Horiz. (0°)	Horiz. (90°)	
Case 1-1 	●	✕	✕	✕	●	✕
Case 1-2 	▲	▲	▲	▲	●	●
Case 2-1 	▲	▲	✕	✕	●	✕
Case 2-2 	✕	●	▲	▲	●	●
Case 3-3 	✕	●	●	●	▲	●

vertical electrode in the TX and horizontal electrode with longitudinal direction in the RX is the optimal choice for BCC.

V. FREQUENCY RESPONSE MODEL AND REFERENCE DISTANCE

To verify the applicability of the theoretical analysis with the measurement results to a real BCC environment, we derive the frequency response model through the theoretical transfer function of (21) and perform the data fitting based on the least root mean square method to the measured data. Since the wavenumber $k(= 2\pi/c_0)$ is proportional to the operating frequency where c_0 is the speed of light ($3 \cdot 10^8$ m/s), and the operating frequency of BCC is below 100 MHz, the value of the wavenumber is smaller than 1 in the frequency of interest. Therefore, the second and third terms of (16) are dominant over the first term of (16), and consequently, we can approximate the electric field intensity in (16) with the following equation:

$$|E(r, k)| = \left| A \cdot k \cdot \frac{1}{r} + i \cdot B \cdot \frac{1}{r^2} - C \cdot \frac{1}{k} \cdot \frac{1}{r^3} \right| \approx \left| i \cdot B \cdot \frac{1}{r^2} - C \cdot \frac{1}{k} \cdot \frac{1}{r^3} \right|. \quad (24)$$

From (24), the transfer function of BCC is expressed in the following form:

$$|H(r, k)| = \frac{|E_{RX}(r, k)|}{|E_z^v(r_0, k)|} \approx \frac{\left| i \cdot B \cdot \frac{1}{r^2} - C \cdot \frac{1}{k} \cdot \frac{1}{r^3} \right|}{2 \cdot \left| i \cdot \frac{1}{r_0^2} - \frac{1}{k} \cdot \frac{1}{r_0^3} \right|} = \frac{\left| i \cdot k \cdot B \cdot \frac{1}{r^2} - C \cdot \frac{1}{r^3} \right|}{2 \cdot \left| i \cdot k \cdot \frac{1}{r_0^2} - \frac{1}{r_0^3} \right|}. \quad (25)$$

As we mentioned in the previous section, Case 1-2 is the optimal configuration for BCC, and we focus on the frequency response model and data fitting for Case 1-2 in this section. Since the value of C in (25) is equal to 0 in Case 1-2, we can obtain the frequency response model with respect to the variable of frequency f as follows:

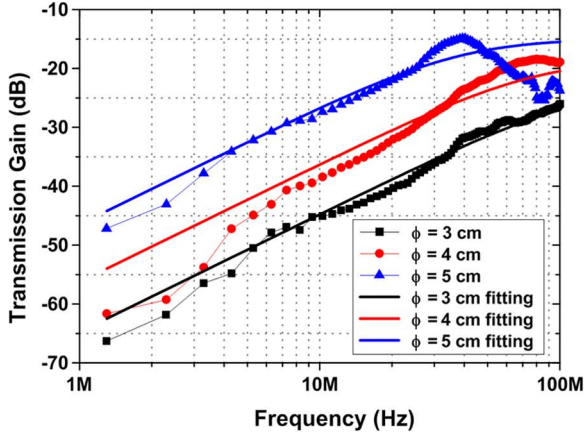
$$|H_{BCCC}(f)| = \left| \frac{i \cdot 2\pi \cdot \frac{B}{c_0} \cdot \frac{1}{r^2} \cdot f}{2 \left(i \cdot 2\pi \cdot \frac{1}{c_0} \cdot \frac{1}{r_0^2} \cdot f - \frac{1}{r_0^3} \right)} \right| = \left| \frac{i \cdot 2\pi \cdot \frac{B}{c_0} \cdot \frac{r_0^3}{r^2} \cdot f}{2 \left(1 - i \cdot 2\pi \cdot \frac{r_0}{c_0} \cdot f \right)} \right| = \left| \frac{\frac{B}{2} \cdot \frac{r_0^2}{r^2} \cdot i \cdot 2\pi \cdot \frac{r_0}{c_0} \cdot f}{1 - i \cdot 2\pi \cdot \frac{r_0}{c_0} \cdot f} \right| = \left| \frac{N \cdot i \cdot M \cdot f}{1 - i \cdot M \cdot f} \right| \quad (26)$$

where $N = (B/2) \cdot (r_0^2/r^2)$ and $M = 2\pi \cdot (r_0/c_0)$. It should be noted that (26) intrinsically has the feature of high-pass filter characteristics, which has a 3-dB cutoff frequency at the $1/M(= (1/2\pi) \cdot (c_0/r_0))$ Hz and a passband gain of $N(= (B/2) \cdot (r_0^2/r^2))$. Furthermore, it is noteworthy that when we set the value of reference distance r_0 to be small, not only does the cutoff frequency increase, but also the passband gain decreases in (26) of the frequency response model, which implies the reference distance r_0 can be a significant design parameter to determine the characteristics of the frequency response, such as the cutoff frequency and the passband gain of BCC. The effects of the reference distance on the channel characteristics closely resemble the influence of the electrode size in the measurement results in Fig. 8.

Accordingly, by means of (26), we suggested the effective and useful design parameter with the reference distance r_0 , and then we found out the relationship between the reference distance and the electrode size using the equivalent reference distance. To obtain the equivalent reference distance from the measurement data, the following equation for the data fitting is exploited based on (26):

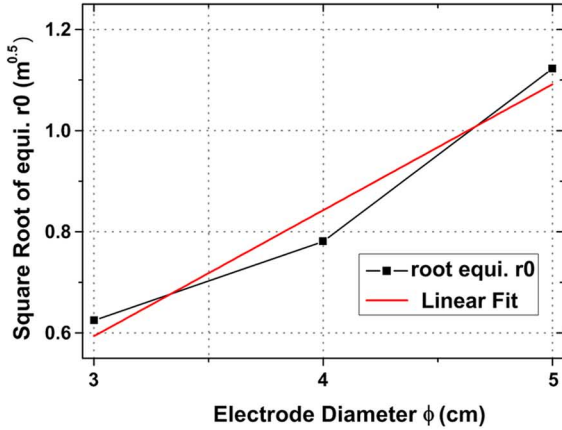
$$y = \frac{N \cdot M \cdot x}{\sqrt{1 + M^2 x^2}}. \quad (27)$$

To fit (27) into the measurement results, the coefficient value of N is found by the maximum passband gain from the measured transmission gain, and then the data are fitted into (27) for extracting the coefficient value of M by the least square approximation method. Fig. 9(a) shows the data fitting results along with the measured data when the channel distance is 0.5 m, and the electrode diameters (ϕ) of 3, 4, and 5 cm are utilized. The coefficient values of M and N , root mean square error (RMSE) value, and the cutoff frequency value, which can be calculated by $1/M$ are listed in Fig. 9(a). As a result, we can derive the value of the equivalent reference distance r_0 from the relation between the coefficient r_0 and $M(r_0 = (1/2\pi) \cdot (M/C_0))$. As found in Fig. 9(a), we noticed that, as the diameter (ϕ) of the electrode increases, the equivalent distance r_0 also increases. Moreover, we found that there is a linear relationship between



	M	N	RMSE	Cutoff Frequency	Equivalent r_0
$\phi = 3$ cm	8.251E-9	0.18	1.153	121.2 MHz	0.39 m
$\phi = 4$ cm	1.279E-8	0.12	2.705	78.2 MHz	0.61 m
$\phi = 5$ cm	2.639E-8	0.07	1.749	37.9 MHz	1.26 m

(a)



Equation	$y = a + b \cdot x$		
Adj. R-Square	0.91209		
		Value	Standard Error
a	Intercept	-0.15332	0.21796
b	Slope	0.249	0.05339

(b)

Fig. 9. Data fitting. (a) With frequency response model with respect to the electrode diameter. (b) Relation between the electrode diameter and the equivalent r_0 .

the square root of the equivalent reference distance ($\sqrt{r_0}$) and the electrode diameter (ϕ), as shown in Fig. 9(b), which means the reference distance is proportional to the area of the electrode.

Lastly, we formulated the relation between the new parameter r_0 in meters and the electrode diameter (ϕ) in centimeters. According to the result of the linear fit in Fig. 9(b), the formula is obtained in (28) for the purpose of proper electrode utilization to determine the suitable electrode size with respect to the required frequency response,

$$\phi = 4.02 \cdot (\sqrt{r_0} + 0.15). \quad (28)$$

Thanks to the theoretical analysis, measurement results, frequency response model, and the parameter r_0 , we can provide a few guidelines for electrode utilization in the design of BCC

systems and many potential applications. First, the optimal electrode usage is the TRX configuration of Case 1-2. Second, we can get the parameter r_0 for the required frequency response of BCC based on transfer function model of (26). Finally, we can properly choose the electrode size using the empirical formula of (28).

VI. CONCLUSION

The effects of electrode configurations on BCC characteristics have been studied for proper electrode utilization in the design of BCC systems and many potential applications. The nine electrode configurations according to the arrangement and direction of both transmitting and receiving electrodes on the body are matched to vertical and horizontal electric dipole sources and receiving components of the z -, r -, and ϕ -directions. We have investigated the theoretical analysis by means of complete equations of electric field intensity and the frequency response of BCC. The theory was validated by both numerical analysis and measurement results, comparing each electrode configuration. In addition, the influence of BCC and RF interferers on the body channel is addressed along with horizontal and vertical RX electrode configurations. Furthermore, to gain an engineering insight about the possible electrode usage, the frequency response model is developed with a reference distance, which is a useful design parameter for the design of BCC systems.

In conclusion, we provide two contributions for the proper electrode utilization in BCC. First, when taking account of the characteristics of the electrode configurations in regard to transmission gain, environmental sensitivity, and interference resilience, Case 1-2, which represents a vertical electrode in the TX and horizontal electrode with the longitudinal direction in the RX, is the optimal electrode usage. Second, we can take advantage of the BCC frequency model developed with the useful parameter that is equivalent reference distance to determine the suitable electrode size for the required frequency response of BCC.

ACKNOWLEDGMENT

The authors would like to thank to J. Jang, M. Kim, and S. Kang, all with the Korea Advanced Institute of Science and Technology (KAIST), Daejeon, Korea, for their helpful measurement support.

REFERENCES

- [1] L. Atzori, A. Iera, and G. Morabito, "The Internet of Things: a survey," *Comput. Netw.*, vol. 54, no. 15, pp. 2787–2805, Oct. 2010.
- [2] B. Latre, B. Braem, I. Moerman, C. Blondia, and P. Demeester, "A survey on wireless body area networks," *Wireless Netw.*, vol. 17, no. 1, pp. 1–18, Jan. 2011.
- [3] *Local and Metropolitan Area Networks—Part 15.6: Wireless Body Area Networks*, IEEE Standard 802.15.6-2012, Feb. 2012, pp. 1–271.
- [4] J. Bae, K. Song, H. Lee, H. Cho, and H.-J. Yoo, "A 0.24 nJ/b wireless body-area-network transceiver with scalable double-FSK modulation," *IEEE J. Solid-State Circuits*, vol. 47, no. 1, pp. 310–322, Jan. 2012.
- [5] J. Bae, K. Song, H. Lee, H. Cho, and H.-J. Yoo, "A low-energy crystal-less double-FSK sensor node transceiver for wireless body-area network," *IEEE J. Solid-State Circuits*, vol. 47, no. 11, pp. 2678–2692, Nov. 2012.
- [6] H. Lee, K. Lee, S. Hong, T. Roh, J. Bae, and H.-J. Yoo, "A 5.5 mW IEEE-802.15.6 wireless body-area-network standard transceiver for multichannel electro-acupuncture application," in *IEEE Int. Solid-State Circuits Conf. Tech. Dig.*, Feb. 2013, pp. 452–453.

- [7] Z. Lucev, I. Krois, and M. Cifrek, "A capacitive intrabody communication channel from 100 kHz to 100 MHz," *IEEE Trans. Instrum. Meas.*, vol. 61, no. 12, pp. 3280–3289, Dec. 2012.
- [8] M. A. Callejon, D. N. Hernandez, J. R. Tosina, and L. M. Roa, "A comprehensive study into intrabody communication measurements," *IEEE Trans. Instrum. Meas.*, vol. 62, no. 9, pp. 2446–2455, Sep. 2013.
- [9] J. Wang, Y. Nishikawa, and T. Shibata, "Analysis of on-body transmission mechanism and characteristic based on an electromagnetic field approach," *IEEE Trans. Microw. Theory Techn.*, vol. 57, no. 10, pp. 2464–2470, Oct. 2009.
- [10] J. Bae, H. Cho, K. Song, H. Lee, and H.-J. Yoo, "The signal transmission mechanism on the surface of human body for body channel communication," *IEEE Trans. Microw. Theory Techn.*, vol. 60, no. 3, pp. 582–593, Mar. 2012.
- [11] J. D. Kraus and R. J. Marhefka, *Antennas*, 3rd ed., Singapore: McGraw-Hill, 2001.
- [12] K. A. Norton, "The propagation of radio waves over the surface of the earth and in the upper atmosphere—Part 1," *Proc. IRE*, vol. 24, no. 10, pp. 1367–1387, Oct. 1936.
- [13] K. A. Norton, "The propagation of radio waves over the surface of the earth and in the upper atmosphere—Part 2," *Proc. IRE*, vol. 25, no. 9, pp. 1203–1236, Sep. 1937.
- [14] S. Gabriel, R. W. Lau, and C. Gabriel, "The dielectric properties of biological tissues: II. Measurements in the frequency range 10 Hz to 20 GHz," *Phys. Med. Biol.*, vol. 41, pp. 2251–2269, Nov. 1996.
- [15] N. Cho, J. Yoo, S. Song, J. Lee, S. Jeon, and H.-J. Yoo, "The human body characteristics as a signal transmission medium for intrabody communication," *IEEE Trans. Microw. Theory Techn.*, vol. 55, no. 5, pp. 1080–1086, May 2007.
- [16] J. Sakai, L.-S. Wu, H.-C. Sun, and Y.-X. Guo, "Balun's effect on the measurement of transmission characteristics for intrabody communication channel," presented at the IEEE MTT-S Int. RF Wireless Technol. Biomedical Healthcare Appl. Workshop, Dec. 2013.



Joonsung Bae (M'14) received the B.S., M.S. and Ph.D. degrees in electrical engineering from the Korea Advanced Institute of Science and Technology (KAIST), Daejeon, Korea, in 2007, 2009, and 2013, respectively. His Ph.D. research concerned wireless body area network (WBAN) circuits and systems.

In 2012, he was a Visiting Scholar with IMEC, Leuven, Belgium, where he researched noise analysis of the dry electrode for body channel communication. From 2013 to 2014, he was with Memory Business, Samsung Electronics, Hwaseong, Korea, where

he developed system-on-chip (SoC) Design for the solid-state drive (SSD) and universal flash storage (UFS). As a Senior Engineer, he designed the integrated circuits for PCI-Express 3.0 and M-PHY 3.0. In 2014, he joined the Information and Electronics Research Institute, KAIST, where he is currently a Postdoctoral

Researcher. His current research interests are high-speed serial interface PHY, short-range wireless connection, WBAN circuits and systems, and biomedical circuits and systems.

Dr. Bae was the recipient of the Asian Solid-State Circuits Conference (A-SSCC) Best Design Award in 2011 and the Global Internship Scholarship of National Research Foundation of Korea in 2012.



Hoi-Jun Yoo (M'95–SM'04–F'08) received the B.S. degree in electronics from Seoul National University, Seoul, Korea, in 1983, and the M.S. and Ph.D. degrees in electrical engineering from the Korea Advanced Institute of Science and Technology (KAIST), Daejeon, Korea, in 1985 and 1988, respectively.

Since 1998, he has been a faculty member with the Department of Electrical Engineering, KAIST, where he is currently a Full Professor. From 2001 to 2005, he was the Director of the Korean System Integration and IP Authoring Research Center (SIPAC). From 2003 to 2005, he was the full-time Advisor to the Minister of Korea Ministry of Information and Communication and National Project Manager for System-on-Chip (SoC) and Computer. In 2007, he founded the System Design Innovation and Application Research Center (SDIA), KAIST. Since 2010, he has been the General Chair of the Korean Institute of Next Generation Computing. He coauthored *DRAM Design* (Hongleung, 1996), *High Performance DRAM* (Sigma, 1999), *Networks on Chips* (Morgan Kaufmann, 2006), *Low-Power NoC for High-Performance SoC Design* (CRC, 2008), *Circuits at the Nanoscale* (CRC, 2009), *Embedded Memories for Nano-Scale VLSIs* (Springer, 2009), *Mobile 3D Graphics SoC from Algorithm to Chip* (Wiley, 2010), and *Bio-Medical CMOS ICs* (Springer, 2011). His current research interests are computer-vision SoC, body area networks, and biomedical devices and circuits.

Dr. Yoo has served as a member of the Executive Committee, ISSCC, Symposium on VLSI, and A-SSCC, and the Technical Program Committee (TPC) chair of A-SSCC 2008 and ISWC 2010. He was an IEEE Distinguished Lecturer (2010–2011), Far East chair of ISSCC (2011–2012), Technology Direction Sub-Committee chair of ISSCC (2013), and Vice TPC chair of ISSCC (2014). He is currently TPC chair of ISSCC (2015). He was the recipient of the Electronic Industrial Association of Korea Award for his contribution to DRAM technology (1994), Hynix Development Award (1995), the Korea Semiconductor Industry Association Award (2002), the Best Research of KAIST Award (2007), the Scientist/Engineer of this Month Award of the Ministry of Education, Science and Technology of Korea (2010), the Best Scholarship Award of KAIST (2011), and Order of Service Merit from the Ministry of Public Administration and Security of Korea (2011). He was a corecipient of the ASP-DAC Design Award (2001), the Outstanding Design Award (2005, 2006, 2007, 2010, 2011 A-SSCC), and the Student Design Context Award (2007, 2008, 2010, 2011 DAC/ISSCC).